Experimental and CFD analyses of a thermal radiation shield dimple plate for cryogenic pump application

2015 IOP Conf. Ser.: Mater. Sci. Eng. 101 012068

(http://iopscience.iop.org/1757-899X/101/1/012068)

IOP Conf. Series: Materials Science and Engineering **101** (2015) 012068 doi:10.1088/1757-899X/101/1/012068

Experimental and CFD analyses of a thermal radiation shield dimple plate for cryogenic pump application

M Scannapiego, C Day
Karlsruhe Institute of Technology, Institute for Technical Physics, Hermann-von-Helmholtz-Platz 1, 76344, Eggenstein-Leopolshafen, Germany

E-mail: matthieu.scannapiego@kit.edu

Abstract. Large customized cryogenic pumps are used in fusion reactors to evacuate the plasma exhaust from the torus. Cryopumps usually consist of an active pumping surface area cooled below 5 K and shielded from direct outer thermal radiation by plates cooled at 80K. In nuclear fusion applications, cryopumps are exposed to excessively high heat fluxes during pumping operation, and follow-up regeneration cycles with rapid warm-up and cool-down phases. Therefore, high cryogenic operational mass flows are required and thus pressure drop and heat transfer characteristics become key issues for the design of the pump cryogenic circuits. Actively cooled dimple plates are a preferred design solution for the thermal radiation shield. A test plate with a rhomb pattern of dimples has been manufactured and tested in terms of pressure drop with a dedicated test facility using water. In the present work, computational fluid dynamics (CFD) models of the test dimple plate have been performed, and computed pressure drops have been compared to experimental results. Despite the complexity of the geometry, a good agreement with the experimental results was found. Then, the validated CFD approach has been further extended to relevant operation conditions, using gaseous helium at cryogenic temperature as working fluid. The resulting pressure drop and heat transfer characteristics are finally presented.

1. Introduction

In order to maintain the required pressure levels in the torus plasma chamber of a thermonuclear fusion reactor and hence to provide a good energy confinement of the plasma, very high gas throughputs have to be processed with a powerful and high speed cryogenic pumping system. Since no commercial solution exists for the very specific requirements of a fusion reactor exhaust pumping system – namely very high pumping speeds for light gases, such as hydrogen species and helium, at moderate vacuum, in a nuclear environment with high magnetic and radiation fields – large customized cryogenic pumps are used. Over the past two decades, the Karlsruhe Institute of Technology (KIT) has developed a broad experience in designing large tailor-made cryogenic pumps for fusion devices. In particular, KIT was charged by ITER to provide the detailed design of the torus exhaust cryopumps as well as the neutral beam injector cryopumps [1-3]. A model pump to prove the suitability of cryogenic pumps for ITER was also previously developed [4,5].

Cryopumping relies on sorption of light gases on activated charcoal [6]. Although very different in size and geometrical arrangement depending on the specific requirements, cryopumps basically consist of active charcoal coated pumping surfaces cooled below 5 K by a supercritical helium forced flow. To prevent from direct outer casing thermal radiation, the 5 K surfaces are tightly surrounded by shields and baffles cooled by a gaseous helium forced flow at about 80 K. 80 K surfaces also provide a

first stage pumping for heavy gases and impurities. During nominal pumping operation, cryopumps are exposed to excessively high heat fluxes. Cryopumps also undergo frequent staggered sequential regenerations at 100 K in order to prevent from saturation, hydrogen deflagration safety hazards, and build-up of tritium inventories [7]. Less frequently, they are regenerated at 300 K and 475 K in order to release air-likes species, and water and hydrocarbons respectively [8,9]. Due to the high heat loads and the limited time to perform regeneration cycles, high cryogenic operating mass flows are required, hence pressure drop and heat transfer are key issues for the design of the pump cryogenic circuits.

For optimal flow distribution and enhanced heat transfer, hydroformed dimple plates are a preferred design solution for the thermal radiation shield components. A test plate with a diamond pattern of dimples has been manufactured, procured, and tested for pressure drop at the KIT with a dedicated test facility using a water loop. The objective of the work presented in this paper was to gain confidence in the ability of a CFD approach to simulate with a satisfactory accuracy flows in this kind of components, before eventually extending the method to other cryopump components. For this purpose, CFD simulations of the test dimple plate are presented and the computed pressure drops compared to the experimental results in order to validate the model. In a second step, the tried and tested CFD method with water is further extended to relevant operation conditions, using helium at cryogenic temperature as working fluid.

2. Pressure drop test facility and test dimple plate

2.1. Pressure drop test facility

Due to the complexity of the internal fluid geometry of the hydroformed components, it is not possible to precisely assess the pressure drop coefficients using literature correlations. Fully relying on a CFD model without crosschecking experimental results beforehand would be also a risky decision. Therefore, the dedicated test facility THEA (Thermal-Hydraulic Experimental Arrangement) was built at the KIT (see figure 1) in order to characterize the coefficients of hydraulic resistance using forced water flows [3,10].

The hydraulic resistance for a given geometry is directly governed by the fluid motion, characterized by the Reynolds number (*Re*) – ratio of inertial forces to viscous forces – and not by the fluid properties themselves. Therefore, pressure drop coefficients obtained with water at defined *Re* can be applied to helium flows at any temperature at the same *Re*, as long as the homogeneous and incompressible flow assumptions hold. THEA was designed to cover the *Re* range found in cryopump components under relevant operation conditions (*Re* range from 6.9×10^3 to 4.8×10^4 is covered in the case of the dimple plate). A heater is placed in the water tank in order to decrease the water viscosity and hence extending the *Re* range.

2.2. Thermal radiation shield test dimple plate

A dimple plate (see figure 1) has been manufactured to be tested for pressure drop. It is made of two 2 mm thickness stainless steel sheets of 2310 mm length and 520 mm width (total weight ~40 kg), laser welded over each other and inflated to a maximal internal height of 8 mm by pressurized water. Due to the presence of patterned welding spots, a complex flow domain is formed, aiming at increasing the flow path across the plate for a better flow distribution and enhanced heat transfer.

The inlet and outlet piping are manually welded at both ends of the panel length. The size of the plate, the dimple rhomb pattern, and the inlet and outlet piping design are representative of thermal radiation shield components used for the customized cryopumps. The presence of the circular welding spots and the distance between them is not only dictated by thermal-hydraulic considerations but they do also provide the required mechanical resistance against over pressurization (required design and burst pressures of 2.1 MPa and 16 MPa respectively).

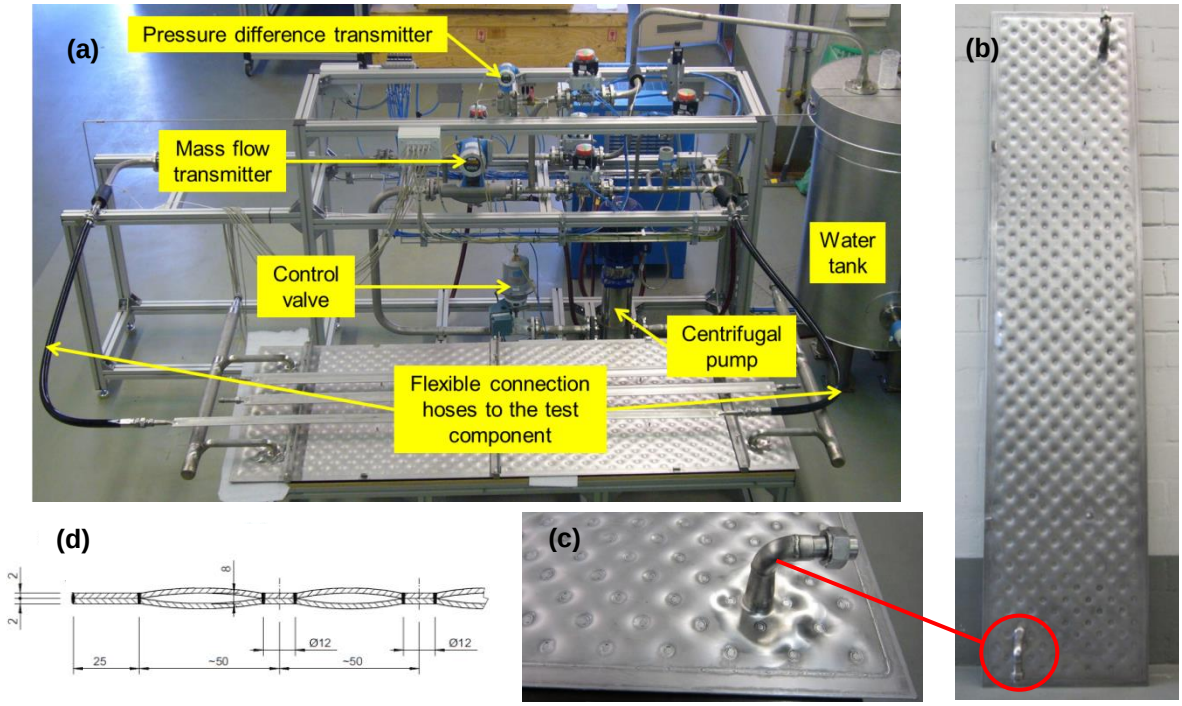

Figure 1. THEA test facility (a), thermal radiation shield test dimple plate (b), detail of the inlet/outlet piping (c), and sketch of the dimple plate cross section (d).

3. CFD model of the dimple plate

3.1. Geometry

The fluid domain geometry is designed using the *Wireframe Surface and Design* module of CATIA V5 in order to create convex surfaces. The domain is then divided in blocks suitable for generating a structured mesh throughout the whole domain, which is basically divided in two regions: the boundary layer region close to the walls and the core flow region (see section 3.3 and figure 2).

3.2. Turbulence modelling and near wall treatment

The CFD analysis is carried out using the commercial code ANSYS CFX. The flow is assumed to be turbulent for the complete *Re* range covered ($6.9\text{x}10^3$ – $4.8\text{x}10^4$). The Reynolds Averaged Navier-Stokes (RANS) two-equation eddy viscosity turbulence model *k-ω Shear Stress Transport (SST)* is used [11]. The *SST* model includes a blending between the *k-ω* (*k* is the turbulence kinetic energy and *ω* the turbulent frequency) model near the surface and the *k-ε* (*ε* is the turbulent eddy dissipation) model in the turbulent layer. The low-Reynolds formulation is used for mesh points located in the viscous sublayer (at dimensionless distance from the wall $y+ < 5$) to solve the details of near wall region with fine near wall grids, which is recommended for accurate pressure drop and heat transfer prediction. When the cells are located in the logarithmic region ($y+ > 30$), wall functions are used. In the buffer layer ($5 < y+ < 30$) where viscosity and turbulence effects are balanced, CFX uses an automatic near wall treatment that ensures a smooth transition between the linear velocity profile in the viscous sublayer and the logarithmic velocity profile. This hybrid near wall treatment is particularly well adapted for the dimple plate complex geometry where significant velocity variations depending on the location are observed, whereas a computational grid resulting in a uniform $y+$ value is impossible to achieve. Moreover one single mesh can be used for a wide range of *Re*.

The stainless steel sheet surfaces of the dimple plate undergo a pickled and passivated treatment and the walls are considered hydraulically smooth.

3.3. Computational grid

ANSYS Mechanical APDL is used to generate a fully hexahedra element structured mesh (see figure 2) for a good grid orthogonality to the fluid flow. In order to take full advantage of the *SST* model near wall low-Reynolds formulation, average $y+$ values close to 1 were targeted, but too small values of $y+$ resulted in numerical instabilities. The boundary layer is built with 15 layers and an expansion factor of 1.15. The resulting average $y+$ value over the plate is in the range of 1.4 – 7.5 for a corresponding *Re* range of $6.9 \times 10^3 – 4.8 \times 10^4$.

A grid sensitivity study was conducted separately for the core mesh. Above ~7×10^6 cells, a further increase of the mesh size of 37 % (9.1×10^6 elements) resulted in less than 0.4 % difference on the total pressure drop, deeming the solution as grid independent. The final mesh used for the calculations presented herein has core mesh elements with a maximal characteristic length of ~1.8 mm for a total count of ~7×10^6 elements.

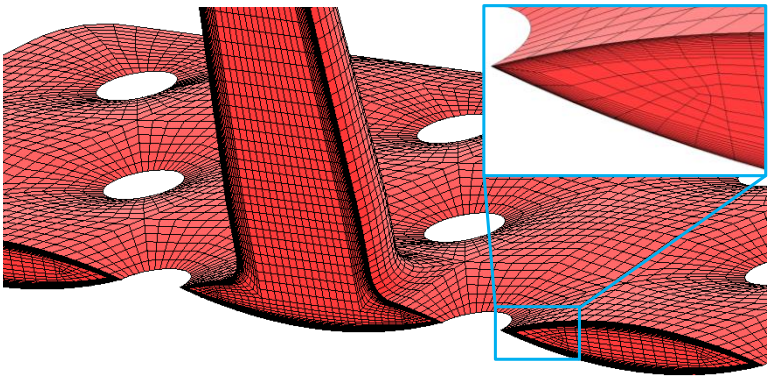

Figure 2. Overview of the computational grid in the inlet/outlet piping region.

4. Validation of the model

The first step of the work is to demonstrate the ability of the CFD model to simulate properly this type of flow by comparing the computed pressure drops with the experimental results obtained from THEA. The validation case is performed with water at 77 °C, for flow rates from 0.5 kg/s to 3.5 kg/s, corresponding to *Re* from 6.9×10^3 to 4.8×10^4.

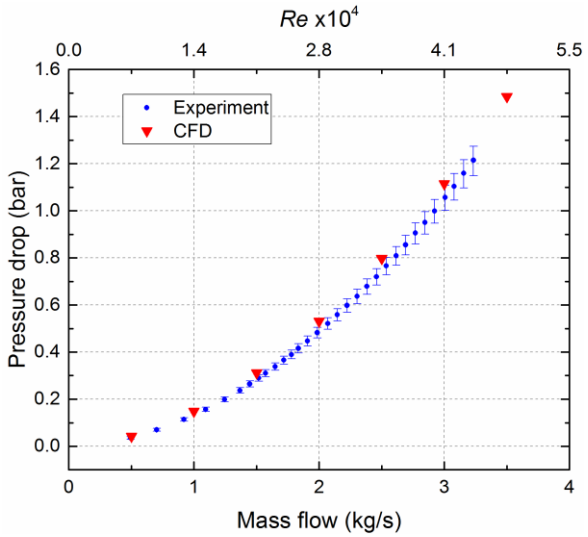

Figure 3. Computed vs. measured pressure drops with water at 77 °C.

The water properties computed by CFX are based on the IAPWS-IF97 formulation (International Association for the Properties of Water and Steam – Industrial Formulation 1997) [12].

As shown in figure 3, the computed pressure drops are in a good agreement with the experimental results, although a slight overestimation is found. This deviation is reduced with increased *Re* (~11% at 1 kg/s, but ~6 % at 3 kg/s).

Here, it is important to mention that the geometry is strictly modeled according to the drawings, but due to the hydroforming process, discrepancies exist between the real geometry and the drawings, which are difficult to take into account in a numerical model. This represents one of the potential sources of errors amongst others (numerical errors and modeling errors). Nonetheless, for our engineering application, a very high level of accuracy is not a requirement and the agreement is judged good enough to demonstrate the applicability of the CFD method for these types of flows.

5. CFD thermal-hydraulic analysis with 80 K gaseous helium

The tried and tested CFD method validated with water is extended to helium flows in relevant operation conditions. In nominal pumping operation, the thermal radiation shields and baffles are cooled by a gaseous helium forced flow at an absolute pressure of about 1.8 MPa. The inlet and maximal outlet temperatures are about 80 K and 90 K respectively. Additionally to the validation case with water, the convective heat transfer coefficients are also characterized. The CFD model could not be validated for heat transfer coefficients against experimental data, but we are confident that the accurate results obtained for the pressure drop calculations provide a good indicator of a well resolved boundary layer, and thus an accurate heat transfer prediction as well.

5.1. CFD model set-up

The simulations with helium are covering the same *Re* range previously investigated with water, therefore the same turbulence model and computational grid is used. Additionally to the continuity and momentum equations, the energy equation is solved.

During nominal pumping operation, thermal radiation is the dominant source of heat load to the cryopump and the outer surface of the cryopump directly exposed to the thermal radiation from room temperature surfaces surrounding the pump is taking over a dominant part of the total heat load. During the cryopump regeneration, the heat fluxes are more balanced between the outer and inner sides of the thermal shields. Therefore, two extreme cases are investigated: in case 1, a homogeneous heat flux of 250 W/m² is imposed on both sides of the plate; in case 2, a homogenous heat flux of 500 W/m² is imposed only over one side of the dimple plate (“outer” side), whereas the other side is set as adiabatic (“inner” side). Each side of the plate having a surface area of about 1.02 m², it results in a total heat load of ~510 W in both cases.

Mass flow rates from 20 g/s to 80 g/s corresponding to a *Re* range of $1.2\text{x}10^4$ – $4.6\text{x}10^4$ are computed.

For simplification purposes, the model does not include the stainless steel domain, and constant helium thermal-physical properties, calculated at 80 K and 1.8 MPa with Hepak [13], are used. The temperature and pressure variations are small enough (< 5 K and < 90 mbar) practically over the whole domain and would lead in reality to a maximum variation of ~6 % of the thermal-physical properties. Nevertheless, significant higher temperatures are found in some very small regions of stagnation in the outlet area, close to the plate edges. In reality this effect would be attenuated by the thermal conduction through the stainless steel sheets.

5.2. Hydraulic resistance and convective heat transfer characterization

Hydraulic resistance and heat transfer coefficients can be both characterized as a function of the *Re*. The *Re* is defined as:

$$Re = \frac{\rho v D_h}{\mu} = \frac{\dot{m} D_h}{\mu A_f} \quad (1)$$

where ρ denotes the fluid density, v the velocity, D_h the hydraulic diameter, $\dot{m}$ the mass flow rate, μ the dynamic viscosity, and A_f the flow cross section. D_h (≈ 10.6 mm) and A_f (≈ 2094 mm²) are calculated at the dimple plate middle cross section formed of 7 bean shape passages separated by 6 weld spots (see figure 1 (d)). The hydraulic diameter D_h is defined as follows:

$$D_h = \frac{4A_f}{P} \tag{2}$$

Where P denotes the wetted perimeter. The overall hydraulic resistance coefficient ξ of the dimple plate is defined as:

$$\xi = \frac{2\Delta p}{\rho v^2} = \frac{2A_f^2 \rho \Delta p}{\dot{m}^2} \tag{3}$$

where Δp is the pressure drop across the dimple plate.

The global convective heat transfer coefficient h of the dimple plate can be derived from the energy balance over the whole domain:

$$h = \frac{Q}{A_{hex}(T_w - T_{ref})} \tag{4}$$

where Q denotes the heat load to the dimple plate, A_{hex} the heat exchange surface area between the fluid and the walls, T_w the average wall temperature, and T_{ref} the fluid reference temperature. Once h is characterized, the idea is to apply equation (3) to estimate the average wall temperature depending on the fluid temperature characterized by T_{ref}. Therefore, a representative and simple formulation of the reference temperature that can be calculated analytically is defined as follows:

$$T_{ref} = \frac{T_{He,in} + T_{He,out}}{2} = T_{He,in} + \frac{Q}{2\dot{m}C_p} \tag{5}$$

where $T_{He,in}$ denotes the helium inlet temperature, $T_{He,out}$ the helium outlet temperature, and Cp the helium heat capacity at constant pressure. h is related to Re via the dimensionless Nusselt number Nu – ratio of convection over conduction – and the fluid thermal conductivity λ:

$$h = \frac{\lambda Nu}{D_h} \tag{6}$$

where Nu is a function of the Re.

The computed pressure drop coefficients ξ and Nusselt Nu as a function of the Reynolds number Re are presented in figures 4 and 5.

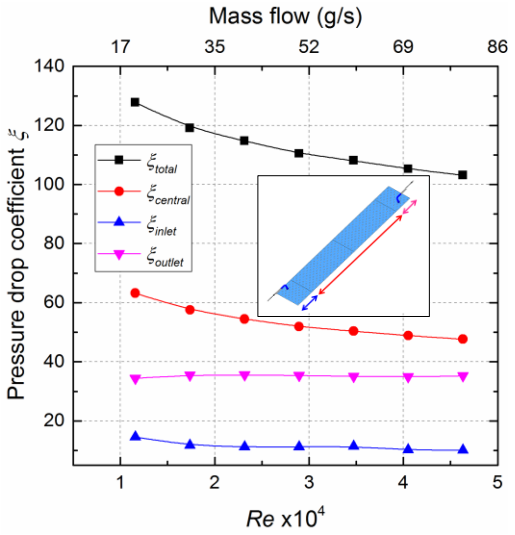

Figure 4. Pressure drop coefficients of the various dimple plate regions (case 1).

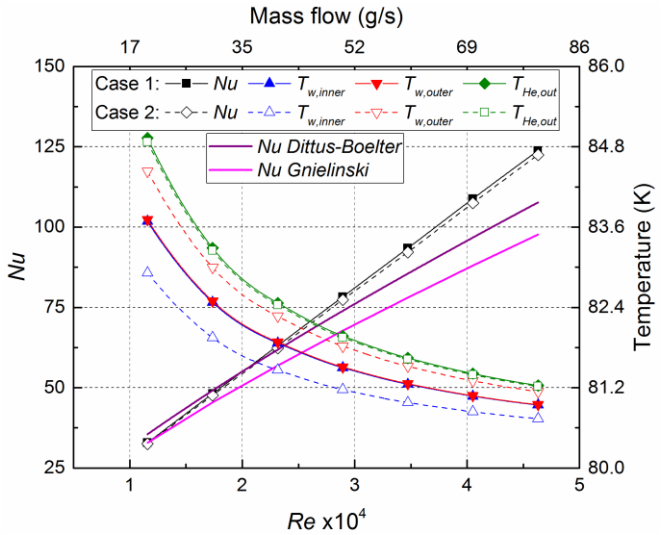

Figure 5. Nusselt number, wall temperatures, and helium outlet temperature for cases 1 and 2.

For more detailed analyses of the pressure drop, the domain is divided in three regions: the plate central region of 1704 mm length (24 patterns of diamond), and the inlet and outlet regions between

the central region and the inlet/outlet of the domain (see the sketch in figure 4). Local pressure drop coefficients are computed for each region ($\xi_{central}$, ξ_{inlet}, and ξ_{outlet}) in order to identify their relative contribution in the overall pressure drop. This provides useful information on the areas where designed could be eventually improved regarding pressure loss reduction. The largest plate central region contributes only to less than 50 % of the overall pressure drop, whereas sudden enlargement/restriction in cross sectional area between the inlet/outlet piping and the plate, and the resulting diverging/converging flows result in high singular pressure losses.

The plate walls are divided into two surfaces ("inner" and "outer") where the average wall temperatures $T_{w,inner}$ and $T_{w,outer}$ are computed. Although $T_{He,out}$ is identical in both cases (the total heat load to the plate is the same), the different heat load distributions result in different wall temperatures between case 1 and case 2, as shown in figure 5. On the other hand, the distribution of the heat load has no impact on the overall heat transfer coefficient. This is to be expected, as constant properties are used for helium. Nevertheless, due to the relative small temperature variations in the domain (and the small thermal-physical properties variations accordingly), particularly in the direction perpendicular to the flow resulting from the thin cross section, different distributions of the heat load are not expected to have a significant effect on the flow motion – and so on the *Re* – and on the *Nu* consequently. As a comparison, the *Nu* given by the Dittus-Boelter and Gnielinski correlations, which are only valid for tubes, are plotted for a circular pipe of diameter 10.6 mm (hydraulic diameter of the dimple plate).

5.3. Analysis of the flow field

An advantage of the CFD technique over the experimental approach is that it gives a complete picture of the thermal-hydraulic of the domain, as shown in figures 6 and 7. A careful analysis of the velocity, pressure, and temperature fields can provide a better understanding of the influence of the geometry on the parameters of interest, namely pressure drop and heat transfer in the present case.

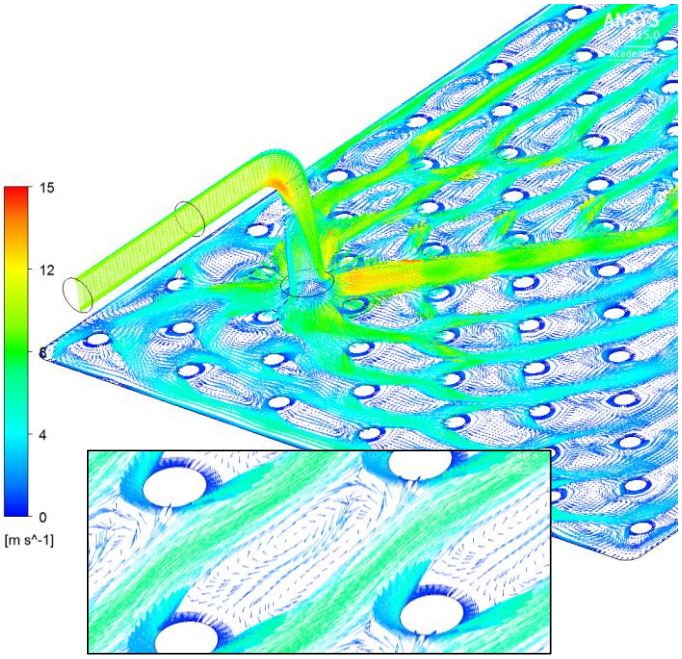

Figure 6. Velocity vector field in the mid-plane of the dimple plate and in a section of the inlet piping at a helium flow rate of 40 g/s.

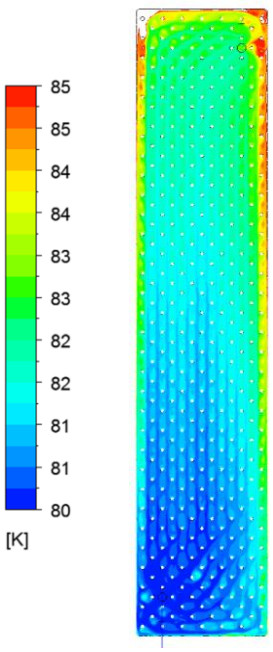

Figure 7. Temperature field in the plate mid-plane at a mass flow rate of 40 g/s and heat flux of 250 W/m² on both sides of the plate (Case 1).

The dimples help spreading efficiently the flow after the inlet piping; hence a homogenous distribution of the cryogen over the complete width of the plate is rapidly developed. Parallel main stream flows are formed between the rows and columns of dimples, moving practically in a straight direction towards the outlet and not taking place in a zig zag manner. Between these high velocity parallel "channels", low velocity vortices are formed in the areas between two successive dimples.

Figure 7 shows that the high flow velocity at the inlet is resulting in locally very high heat transfer coefficients, leading to a rapid increase of the coolant temperature. Due to smaller inflated height close to the edges of the plate – in this region the inflation of the stainless steel sheets is limited by the small gaps between the circular welding spots and the edge welding – the local mass flow is lower than in the centre "channels". As a consequence, the temperature locally increases in these regions.

6. Conclusion and perspective

Despite the complexity of the geometry and the flow motion and taking into account additionally the geometrical irregularities inherent to the hydroforming manufacturing, the computed pressure drops with the CFD technique are in a good agreement with experimental results, thereby validating the CFD model. It was demonstrated that an efficient CFD approach using one single mesh for a broad range of Reynolds could be used with confidence for pressure drop and heat transfer calculations with a satisfactory accuracy, more than sufficient for our engineering application. It represents therefore a good complement or alternative to experiments. Moreover, the CFD approach allows for local and detailed investigation of the flow field. In perspective, CFD constitutes an ideal tool for systematic parametric analyses of some geometrical parameters such as the plate inflated height, the dimples spacing arrangement, or the inlet and outlet piping connections configuration. For accurate heat transfer analyses, models including helium temperature dependent thermal-physical properties and the stainless steel sheets for conjugate heat transfer calculations are foreseen.

7. References

[1] Hauer V, Boissin J C, Day C, Haas H, Mack A, Murdoch D, Lässer R and Wykes M 2007 Design of the ITER prototype cryopump *Fus. Eng. Des.* **82** 2113-2119
[2] Dremel M, Pearce R, Strobel H, Hauer V, Day C, Wikus P and Papastergiou S 2013 The new build to print design of the ITER torus cryopump *Fus. Eng. Des.* **88** 760-763
[3] Day C et al. 2011 Design progress for the ITER torus and neutral beam cryopumps *Fus. Eng. Des.* **86** 2188-2191
[4] Mack A, Day C, Haas H, Murdoch D K, Boissin J C and Schummer P 2001 First operation experience with ITER-FEAT model pump *Fus. Eng. Des.* **58**/**59** 301-306
[5] Haas H, Day C and Mack A, Murdoch D K 2003 Performance tests of the ITER model pump *Fus. Eng. Des.* **69** 91-95
[6] Day C 2001 The use of active carbons as cryosorbent *Colloids Surf. A: Physiochem. Eng. Aspects.* **187**/**188** 187-206
[7] Pearce R J, Antipenkov A, Boussier B, Bryan S, Dremel M, Levesy B, Mayaux C and Wykes M 2013 The ITER divertor pumping system, design evolution, simplification and performance *Fus. Eng. Des.* **88** 809-813
[8] Day C, Kammerer B and Mack A 2000 The influence of water on the performance of ITER cryosorption vacuum pumps *Fus. Eng. Des.* **51-52** 229-235
[9] Day C and Haas H 2009 Experimetal assessment of the ITER cryosorption pump high temperature regeneration *Fus. Eng. Des.* **84** 665-668
[10] Scannapiego M, Day C, Hanke S and Hauer V 2011 Thermohydraulic investigation on the ITER neutral beam injector cryopump *Proceedings of ICEC 23 – ICMC 2010* (Wroclaw, Poland: Wroclaw University of Technology Publishing House) 827-832
[11] ANSY CFX-solver modeling guide and theory guide (Release 15.0)
[12] IAPWS, http://www.iapws.org
[13] CRYODATA, http://www.htess.com/software.htm